

LETTER TO THE EDITOR

EPIC210957318 b and EPIC212110888 b: two inflated hot-Jupiters around Solar-type stars

J. Lillo-Box^{1,2}, O. Demangeon³, A. Santerne^{4,3}, S. C. C. Barros⁴, D. Barrado², G. Hébrard^{5,6}, H. P. Osborn⁷, D. J. Armstrong^{7,12}, J.-M. Almenara^{8,9}, I. Boisse³, F. Bouchy^{3,10}, D. J. A. Brown⁷, B. Courcol⁷, M. Deleuil³, E. Delgado Mena⁴, R. F. Díaz⁷, J. Kirk⁷, K. W. F. Lam⁷, J. McCormac⁷, D. Pollacco⁷, A. Rajpurohit^{3,11}, J. Rey¹⁰, N. C. Santos^{4,13}, S. G. Sousa⁴, M. Tsantaki⁴, P. A. Wilson⁷

¹ European Southern Observatory (ESO), Alonso de Cordova 3107, Vitacura, Casilla 19001, Santiago de Chile (Chile)
e-mail: jlillobox@eso.org

² Depto. de Astrofísica, Centro de Astrobiología (CSIC-INTA), ESAC campus 28692 Villanueva de la Cañada (Madrid), Spain

³ Aix Marseille Université, CNRS, Laboratoire d'Astrophysique de Marseille UMR 7326, 13388, Marseille, France

⁴ Instituto de Astrofísica e Ciências do Espaço, Universidade do Porto, CAUP, Rua das Estrelas, PT4150-762 Porto, Portugal

⁵ Institut d'Astrophysique de Paris, UMR7095 CNRS, Université Pierre & Marie Curie, 98bis boulevard Arago, 75014 Paris, France

⁶ Observatoire de Haute-Provence, Université d'Aix-Marseille & CNRS, 04870 Saint-Michel l'Observatoire, France

⁷ Department of Physics, University of Warwick, Gibbet Hill Road, Coventry, CV4 7AL, UK

⁸ Université Grenoble Alpes, IPAG, 38000 Grenoble, France

⁹ CNRS, IPAG, 38000 Grenoble, France

¹⁰ Observatoire Astronomique de l'Université de Genève, 51 chemin des Maillettes, 1290 Versoix, Switzerland

¹¹ Astronomy and Astrophysics Division, Physical Research Laboratory, Ahmedabad 380009, India

¹² ARC, School of Mathematics & Physics, Queen's University Belfast, University Road, Belfast BT7 1NN, UK

¹³ Depto. de Física e Astronomia, Faculdade de Ciências, Universidade do Porto, Rua Campo Alegre, 4169-007 Porto, Portugal

January 28, 2016

ABSTRACT

We report the discovery of the two hot-Jupiters EPIC210957318 b and EPIC212110888 b (hereafter EPIC-318 b and EPIC-888 b, respectively). The two planets were detected transiting their main-sequence star with periods ~ 4.099 and ~ 2.996 days, in campaigns 4 and 5 of the extension of the *Kepler* mission, K2. Subsequent ground-based radial velocity follow-up with SOPHIE, HARPS-N and CAFE, established the planetary nature of the transiting objects. We analyzed the transit signal, radial velocity and spectral energy distributions of the two systems to characterize their properties. Both planets (EPIC-318 b and EPIC-888 b) are bloated hot-Jupiters ($1.25 R_{\text{Jup}}$ and $1.33 R_{\text{Jup}}$) around relatively bright ($V = 13.5$ and $V = 11.5$), slow rotating main-sequence (G8 and F9) stars. Thus, these systems are good candidates for detecting the Rossiter-MacLaughlin effect to measure their obliquity and for atmospheric studies.

Key words. Planets and satellites: detection, gaseous planets; Techniques: radial velocities, high angular resolution, photometric.

1. Introduction

The extension of the *Kepler* mission (K2, Howell et al. 2014) is photometrically monitoring different fields along the ecliptic in ~ 80 day timespans. Despite the smaller timespan and the slightly lower photometric precision with respect to the prime mission, several tens of extrasolar planets have been detected and characterized so far. These planets cover a wide range of properties, from disintegrating Neptune-size objects (Sanchis-Ojeda et al. 2015) through validated Earth-size planets (e.g. Crossfield et al. 2015; Petigura et al. 2015) to resonant multi-planetary systems (Armstrong et al. 2015b; Barros et al. 2015).

Several works have provided planet candidates based on independent analysis of the light curves (e.g., Foreman-Mackey et al. 2015). However, as in the prime part of the mission, any candidate requires follow-up observations to unveil its nature. Due to the large *Kepler* pixel size (around 4×4 arcsec), contaminant sources can lie within the photometric aperture. Several high-spatial resolution follow-up surveys were carried out for the prime mission (e.g. Lillo-Box et al. 2012, 2014b; Adams et al. 2012; Law et al. 2014) concluding that 20-40% of the can-

didates have stellar companions closer than 3 arcsec. Thus, both high-resolution images and radial velocity (RV) data are needed.

The currently known extrasolar planets show an interesting population of close-in ($a < 0.1$ au) gaseous planets, known as hot-Jupiters (hereafter HJ), with a maximum frequency at a 5-day period (Santerne et al. 2015b). The detection and full characterization of these systems has become crucial to understanding early migration processes as well as planet-star and planet-planet interactions. These are the best targets to study these processes because their consequences are easily detectable from the ground. For instance, HJs were found to be mostly solitary (Steffen et al. 2012), with no other planets in the system. This was explained by possible suppression of rocky planet formation due to the inward migration of the HJ early in the evolution of the system (e.g., Armitage 2003). But, the detection of inner and outer planets to the HJ WASP-47 b using K2 (Becker et al. 2015) has challenged this scenario. Also, measuring the spin-orbit angle provides hints on the migration history of the system (Morton & Johnson 2011) and has been determined for many HJ so far (e.g., Winn et al. 2005). Additionally, many HJs are found to be

bloated. The source of such inflation is still not well understood, and several mechanisms have been proposed (e.g., Batygin & Stevenson 2010; Showman & Guillot 2002). But none can explain the inflation by itself. On top of this, transiting HJs are currently the best chance to study exoplanet atmospheres, and high precision light curves also allow phase curve studies.

Hence, a full characterization of a large population of HJs is necessary to analyze the migration and formation history of these systems as well as study the planet-planet and planet-star interactions. We have used data from different facilities to identify and characterize the extrasolar planets EPIC-888 b and EPIC-318 b, two inflated hot-Jupiters around Solar-like stars. In this paper we detail the observations, data reduction, analysis and conclusions about these systems.

2. Observations and data handling

2.1. K2 photometry

The star EPIC-318 (EPIC210957318, 03:29:22.07 +22:17:57.9) was observed by K2 during its campaign 4, between 2015-02-07 and 2015-04-23. EPIC-888 (EPIC212110888, 08:30:18.91 +22:14:09.3) belongs to field-of-view 5, photometrically monitored by K2 between 2015-04-27 and 2015-07-10. The data was reduced using both the Warwick (Armstrong et al. 2015a) and the LAM- K2 (Barros et al. 2015) pipelines. The detrended data (see Tables A.1 and A.2) show 1.9% and 0.8% dims every 4.099 and 2.996 days for EPIC-318 and EPIC-888, respectively (see Figs. 1 and 2).

2.2. High-spatial resolution imaging

We obtained a high-spatial resolution image of EPIC-888 with the instrument AstraLux at the 2.2m telescope in Calar Alto Observatory (Spain). We used the lucky-imaging technique, obtaining 90 000 frames, each with an exposure time of 0.040 s using the maximum gain setting. The images were reduced with the observatory pipeline, which performs basic reduction of the individual frames, selects the frames with the best Strehl ratios (Strehl 1902), aligns those frames and combines them to provide a final near-diffraction limited image. In this case, we selected the best 10% of frames, which translates into an effective exposure time of 360 s. No companions are detected within the sensitivity limits of the image. The sensitivity curve was obtained by following the prescriptions in Lillo-Box et al. (2014a), simulating artificial stars at different positions in the reduced image and different contrast magnitudes and counting how many of them are recovered with a 5σ signal-to-noise. In summary, the image would have allowed us to detect companions with contrast magnitudes brighter than 3.5 mag at 0.5 arcsec, 5.3 mag at 1 arcsec and 8 mag at 2 arcsec. Since no companion is detected within these limits, we assume that EPIC-888 is isolated and that the light curve is not polluted by other sources. Since no high-resolution image is available for EPIC-318, we checked the 2MASS (Cutri et al. 2003) and SDSS DR9 (Ahn et al. 2012) images and found no companion between 3-10 arcsec. We thus assume that the target is also isolated.

2.3. High-resolution spectroscopy

We observed the two transited stars with HARPS-N (Cosentino et al. 2012) at the Telescopio Nazionale Galileo (TNG, Spain) and SOPHIE (Bouchy et al. 2013) at the Observatoire de Haute-Provence (OHP, France). Two additional epochs for EPIC-888

were obtained with CAFE (Aceituno et al. 2013) at the 2.2m telescope of the Calar Alto Observatory (CAHA, Spain). The three instruments are fiber-fed high-resolution echelle spectrographs with resolving powers of $R \sim 40\,000$ (SOPHIE in the high-efficiency mode), $R = 110\,000$ (HARPS-N) and $R = 63\,000$ (CAFE) and having no movable pieces. They are located in isolated chambers to improve the stability. SOPHIE and HARPS-N are stabilized in temperature and pressure while these ambient conditions are simply monitored in the case of CAFE to check for possible RV drifts. In the three cases, the data was reduced with the corresponding online pipelines¹. The RV is subsequently computed by determining the weighted cross-correlation function (CCF) between the spectra and a G2V binary mask² (Baranne et al. 1996; Pepe et al. 2002). SOPHIE data were corrected from the charge transfer inefficiency present in the charge-couple device of the instrument (Santerne et al. 2012). The RVs were also corrected from instrumental drifts using the RV standard star HD 56124 observed during the same nights and following the prescriptions in Santerne et al. (2014). CAFE RVs were also corrected using observations of the same standard star during the nights.

For EPIC-318, seven epochs were obtained with HARPS-N during four consecutive nights (4-7 January, 2016) and five epochs were obtained with SOPHIE in the subsequent seven nights (8-13 January, 2016). This provides a time span of ten days for this ~ 4 -day period planet. For EPIC-888, we obtained 3 epochs with HARPS-N on 4-7 January 2016, 4 epochs with SOPHIE on 10-15 January 2016, and two epochs with CAFE on 24-25 of December 2015. This encompasses a 22-day time span for this ~ 3 -day period planet. The derived RV values are shown in Tables A.3 and A.4. In both cases, the radial velocity variations show no significant correlation with the bisector values, indicating that they are not originated by blended (undetected) stars. We calculated the projected rotational velocity of the star using the corresponding CCF following Boisse et al. (2010), see Table A.7.

3. Results

3.1. Stellar properties

The spectral analysis was performed on the HARPS-N data. For EPIC-318 the seven spectra were combined, while for EPIC-888 we used a single spectra that presented much higher S/N. The spectroscopic parameters were derived with the ARES+MOOG method (see Sousa 2014, for details) which is based on the measurement of equivalent widths of iron lines with ARES (Sousa et al. 2015). This method has been used to derive homogeneous parameters for planet-host stars (e.g., Santos et al. 2013). The derived properties (T_{eff} , $\log g$, and $[\text{Fe}/\text{H}]$) for this G8V (EPIC-318) and F9V (EPIC-888) were used as priors for the joint analysis of the data (see Sect. 3.2) and are provided in Table A.5. Additionally, we also determined the lithium abundance for these host stars. We found an abundance of $A(\text{Li}) = 2.16 \pm 0.2$ dex for EPIC-888 ($T_{\text{eff}} = 6130 \pm 50$ K) and an upper limit of $A(\text{Li}) < 0.9$ dex for EPIC-318 ($T_{\text{eff}} = 5585 \pm 38$ K). These abundances provide an estimated lower limit for the age of both targets of 2 Gyr when compared to the abundances of members of the NGC752 (Sestito et al. 2004) or M67 cluster (Pasquini et al. 2008).

¹ For the CAFE pipeline, see <http://www.caha.es/CAHA/Instruments/CAFE/software> for details.

² In the case of CAFE, see section 2.3 Lillo-Box et al. (2015).

3.2. Joint analysis of the data

We used the PASTIS software (Díaz et al. 2014; Santerne et al. 2015a) to perform a joint analysis of the K2 light curve, radial velocities, and magnitudes of the two targets. The transit signals were modeled³ using a modified version of the JKTEBOP code (Southworth 2011, and references therein) and RVs were fitted to a Keplerian orbit. The spectral energy distribution (SED, Table A.6) was modeled with the BT-SETTL library (Allard 2014) and the stellar parameters were derived using the Dartmouth stellar evolution tracks (Dotter et al. 2008).

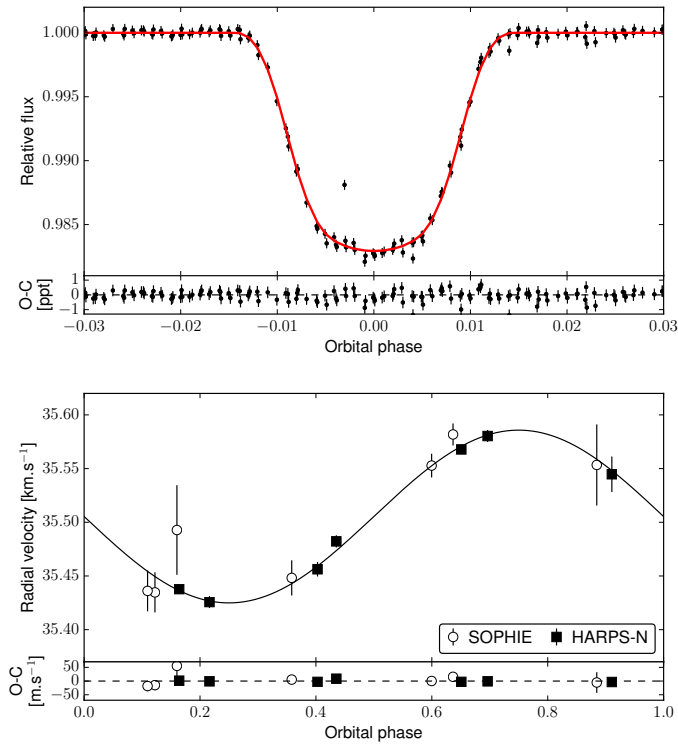


Fig. 1. Results of the joint analysis with PASTIS for EPIC-318, including the primary transit (top panel) and radial velocity (bottom panels). The final models are shown with solid lines and the residuals of the data are presented in the lower part of each panel.

We performed a statistical analysis using Markov Chain Monte-Carlo (MCMC) algorithms. The model is described by six free parameters for the host star (T_{eff} , $\log g$, $[\text{Fe}/\text{H}]$, systemic radial velocity V_{sys} , interstellar extinction $E(B-V)$, and distance d) and seven free parameters for the transit (period P , epoch of first transit T_0 , radial velocity amplitude K , radius ratio R_p/R_* , orbital eccentricity e , inclination i , and argument of periastron ω). For the light curve, we also fit for an additional source of white noise, the out-of-transit flux level, and the level of contamination. For the RV, we additionally fit for a jitter term for each instrument and a RV offset between SOPHIE and the other instruments used. A jitter is also added for the SED analysis. For EPIC-888, due to the low number of RV datapoints, we assumed a circular orbit. This assumption is justified by the short period and circularization mechanisms. In total, 20 free parameters are fitted for both systems. Uniform priors are used for all free parameters except for the stellar values that were constrained to the results of the spectral analysis (see Sect. 3.1). The list of

³ Models are numerically integrated over the *Kepler* exposure time with an oversampling factor of 10.

priors is shown in Table A.5. We ran 20 chains of 3×10^5 iterations randomly drawn from the joint prior distribution. All chains converged toward the same solution which is assumed to be the global maximum. In order to obtain the final solution and its uncertainties, we removed the burn-in phase of each chain and thinned them by computing their maximum correlation length. Then, we merged all of them to compute a well-sampled and clean posterior distribution having more than 2000 independent samples. The median values are presented in Table A.7 together with the 15.7% and 84.3% percentiles of the marginalized distributions. In the table we also present other parameters derived from those fitted by the model (e.g., planet mass, planet radius, stellar mass, etc.). The data and best fit models are presented in Figs 1, 2 and A.1.

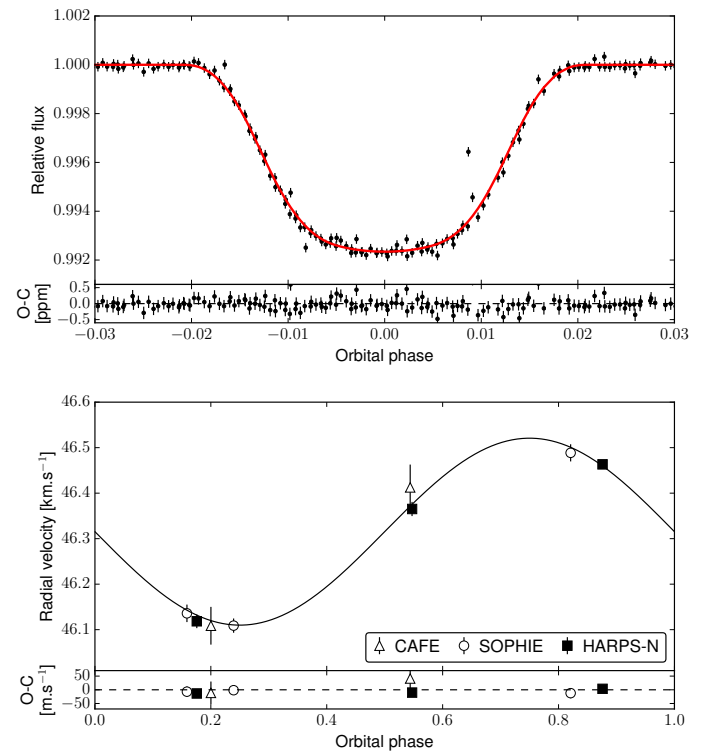


Fig. 2. Results of the joint analysis with PASTIS for EPIC-888. Same symbols as in Fig. 1.

4. Discussion

The combination of different datasets for EPIC-318 b and EPIC-888 b establishes the planetary nature of the transiting objects around two main-sequence stars (G8V and F9V, respectively) observed by K2. The analysis of the data indicate that both systems are composed of single giant ($1.196 \pm 0.060 R_{\text{Jup}}$ for EPIC-318 and $1.350 \pm 0.067 R_{\text{Jup}}$ for EPIC-888) planets in close-in orbits around their main-sequence stars.

In the case of EPIC-318, the insolation flux received by the planet is $F = 4.24 \pm 0.39 \times 10^8 \text{ erg s}^{-1} \text{ cm}^{-2}$. This is significantly larger than the empirical cut off limit derived by Demory & Seager (2011) for a planet to have an inflated radius ($F > 2.08 \times 10^8 \text{ erg s}^{-1} \text{ cm}^{-2}$). Assuming a Bond albedo $A = 0$ and a complete redistribution of the tidal heating along the planet, its expected radius according to Eq. 9 in Enoch et al. (2012) would

be $0.777 \pm 0.015 R_{\text{Jup}}^4$. According to Weiss et al. (2013) the mass-radius-insolation flux provide an expected radius for this planet of $1.150 \pm 0.010 R_{\text{Jup}}$. In the case of EPIC-888 b, this planet receives an insolation flux of $F = 2.07 \pm 0.22 \times 10^9 \text{ erg s}^{-1} \text{ cm}^{-2}$. This is one order of magnitude larger than the above mentioned cut off limit derived by Demory & Seager (2011). The expected radius according to Enoch et al. (2012) would be $1.036 \pm 0.023 R_{\text{Jup}}$ and the expected radius from Weiss et al. (2013) is $1.283 \pm 0.014 R_{\text{Jup}}$.

In both cases, the planets have slightly larger radius than that predicted by empirical calibrations (see Fig. 3). Although compared to the values predicted by Weiss et al. (2013) they are compatible within 1σ with being inflated due to the high stellar insolation flux, both are clearly larger ($> 3\sigma$) than the predicted value by Enoch et al. (2012). It is known that high stellar irradiance can explain the inflation of the close-in Jupiter planets with radius up to $\sim 1.2 R_{\text{Jup}}$ (Guillot & Showman 2002). However, this cannot explain larger radius, and so other mechanisms must play a role (e.g., Bodenheimer et al. 2001; Batygin & Stevenson 2010; Chabrier & Baraffe 2007). The small eccentricity found in EPIC-318 could possibly indicate some tidal heating but other mechanisms cannot be rejected.

In this paper, we have characterized two HJs. They show bloated radii possibly due to the large stellar insolation that they are receiving from their host. However, other possible mechanisms such as tidal heating may be playing a role. Since the hosts are bright ($V = 11.5$ for EPIC-888 and $V = 13.5$ for EPIC-318) and the planets are inflated, they are amenable for atmosphere characterization either from the ground or from space. As they transit, they are also good candidates for the detection of the Rossiter-MacLaughlin effect to infer the spin-orbit angle and study the evolutionary history of these systems. From the derived parameters, the amplitude of this effect should be around 60 m/s and 40 m/s for EPIC-318 and EPIC-888, respectively. Also, the search for additional bodies will be interesting to unveil planet-planet interactions during the onset of the planetary systems.

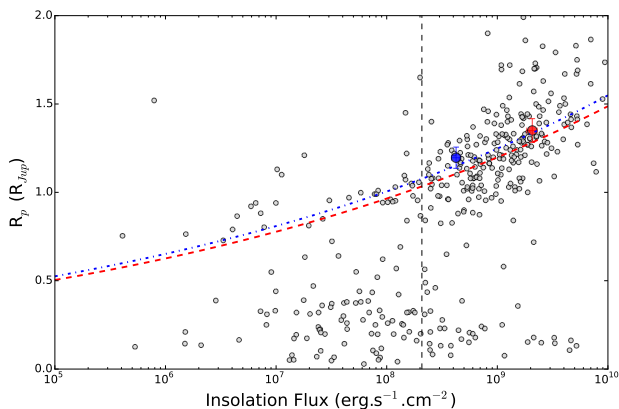


Fig. 3. Insolation flux and planet radius for all extrasolar planets with known radius, T_{eff} and semi-major axis. Data taken from the The Extrasolar Planet Encyclopedia. The two hot-Jupiters found in this work are marked as filled circles (EPIC-888 in red and EPIC-318 in blue). The expected radius-insolation flux dependency for each system according to Weiss et al. (2013) is shown as dashed red (EPIC-888) and dash-dot blue (EPIC-318) lines.

Acknowledgements. J.L-B acknowledges financial support from the Marie Curie Actions of the European Commission (FP7-COFUND) and the Span-

⁴ Larger albedos would imply smaller expected planetary radius so this can be considered as an upper limit.

ish grant AYA2012- 38897-C02-01. O.D. acknowledges support by CNES through contract 567133. A.S. is supported by the European Union under a Marie Curie Intra-European Fellowship for Career Development with reference FP7-PEOPLE-2013-IEF, number 627202. D.J.A. and D.P. acknowledge funding from the European Union Seventh Framework programme (FP7/2007-2013) under grant agreement No. 313014 (ETA-EARTH). J.-M.A. acknowledges funding from the European Research Council under the ERC Grant Agreement n. 337591-ExTrA. P.A.W. acknowledges the support of the French Agence Nationale de la Recherche (ANR), under program ANR-12-BS05-0012 "Exo-Atmos". AS, SCCB, EDM, NCS, SS, and MT acknowledge support by Fundação para a Ciência e a Tecnologia (FCT) through the research grants UID/FIS/04434/2013 (POCI-01-0145-FEDER-007672) and project PTDC/FIS-AST/1526/2014. NCS, SGS, and SCCB acknowledge the support from FCT through Investigador FCT contracts of reference IF/00169/2012, IF/00028/2014, and IF/01312/2014, respectively, and POPH/FSE (EC) by FEDER funding through the program "Programa Operacional de Factores de Competitividade - COMPETE". EDM acknowledges the support from FCT in the form of the grant SFRH/BPD/76606/2011. This publication is based on observations collected with the NASA satellite Kepler, with the SOPHIE spectrograph at OHP (CNRS, France), HARPS-N (La Palma, Spain), and CAFE and AstraLux at Calar Alto Observatory (Spain). This publication makes use of data products from the Wide-field Infrared Survey Explorer, which is a joint project (UCLA/JPL) funded by NASA. This research made use of the AAVSO Photometric All-Sky Survey, funded by the Robert Martin Ayers Sciences Fund.

References

- Aceituno, J., Sánchez, S. F., Grupp, F., et al. 2013, *A&A*, 552, A31
 Adams, E. R., Ciardi, D. R., Dupree, A. K., et al. 2012, *AJ*, 144, 42
 Ahn, C. P., Alexandroff, R., Allende Prieto, C., et al. 2012, *ApJS*, 203, 21
 Allard, F. 2014, in *IAU Symposium*, Vol. 299, *IAU Symposium*, ed. M. Booth, B. C. Matthews, & J. R. Graham, 271–272
 Armitage, P. J. 2003, *ApJ*, 582, L47
 Armstrong, D. J., Kirk, J., Lam, K. W. F., et al. 2015a, *A&A*, 579, A19
 Armstrong, D. J., Santerne, A., Veras, D., et al. 2015b, *A&A*, 582, A33
 Baranne, A., Queloz, D., Mayor, M., et al. 1996, *A&AS*, 119, 373
 Barros, S. C. C., Almenara, J. M., Demangeon, O., et al. 2015, *MNRAS*, 454, 4267
 Batygin, K. & Stevenson, D. J. 2010, *ApJ*, 714, L238
 Becker, J. C., Vanderburg, A., Adams, F. C., Rappaport, S. A., & Schwengeler, H. M. 2015, *ApJ*, 812, L18
 Bodenheimer, P., Lin, D. N. C., & Mardling, R. A. 2001, *ApJ*, 548, 466
 Boisse, I., Eggenberger, A., Santos, N. C., et al. 2010, *A&A*, 523, A88
 Bouchy, F., Díaz, R. F., Hébrard, G., et al. 2013, *A&A*, 549, A49
 Chabrier, G. & Baraffe, I. 2007, *ApJ*, 661, L81
 Cosentino, R., Lovis, C., Pepe, F., et al. 2012, in *Society of Photo-Optical Instrumentation Engineers (SPIE) Conference Series*, Vol. 8446, 1
 Crossfield, I. J. M., Petigura, E., Schlieder, J. E., et al. 2015, *ApJ*, 804, 10
 Cutri, R. M., . . . & et al. 2013, *VizieR Online Data Catalog*, 2328
 Cutri, R. M., Skrutskie, M. F., van Dyk, S., et al. 2003, *VizieR Online Data Catalog*, 2246, 0
 Demory, B.-O. & Seager, S. 2011, *ApJS*, 197, 12
 Díaz, R. F., Montagnier, G., Leconte, J., et al. 2014, *A&A*, 572, A109
 Sanchis-Ojeda, R., Rappaport, S., Pallé, E., et al. 2015b, *ArXiv e-prints*
 Santerne, A., Díaz, R. F., Almenara, J.-M., et al. 2015a, *MNRAS*, 451, 2337
 Santerne, A., Díaz, R. F., Moutou, C., et al. 2012, *A&A*, 545, A76
 Santerne, A., Hébrard, G., Deleuil, M., et al. 2014, *A&A*, 571, A37
 Santerne, A., Moutou, C., Tsantaki, M., et al. 2015b, *ArXiv e-prints*
 Santos, N. C., Sousa, S. G., Mortier, A., et al. 2013, *A&A*, 556, A150
 Sestito, P., Randich, S., & Pallavicini, R. 2004, *A&A*, 426, 809
 Showman, A. P. & Guillot, T. 2002, *A&A*, 385, 166
 Sousa, S. G. 2014, *ArXiv e-prints*
 Sousa, S. G., Santos, N. C., Adibekyan, V., Delgado-Mena, E., & Israelian, G. 2015, *A&A*, 577, A67
 Southworth, J. 2011, *MNRAS*, 417, 2166
 Steffen, J. H., Ragozzine, D., Fabrycky, D. C., et al. 2012, *Proceedings of the National Academy of Science*, 109, 7982
 Strehl, K. 1902, *Astronomische Nachrichten*, 158, 89
 Weiss, L. M., Marcy, G. W., Rowe, J. F., et al. 2013, *ApJ*, 768, 14
 Winn, J. N., Noyes, R. W., Holman, M. J., et al. 2005, *ApJ*, 631, 1215

Table A.1. Normalized detrended K2 light curve of EPIC 210957318 (see Sect. 2.1). The complete version of this table is available online in the CDS.

BJD-2400000 (days)	Flux	Flux unc
2457067.684383	1.000706	0.000103
2457067.704815	0.999879	0.000103
2457067.725247	0.999752	0.000103
2457067.745679	0.999817	0.000103
2457067.766111	0.999762	0.000103
...

Table A.2. Normalized detrended K2 light curve of EPIC 212110888 (see Sect. 2.1). The complete version of this table is available online in the CDS.

BJD (days)	Flux	Flux unc
2457139.630908	0.999991	0.000042
2457139.651340	0.999988	0.000042
2457139.671772	0.999930	0.000042
2457139.692204	0.999910	0.000042
2457139.712636	1.000159	0.000042
...

Table A.3. Radial velocity data for EPIC-210957318

MBJD (days)	RV (km/s)	BIS (m/s)	FWHM (km/s)	Instrument
392.35938	35.5624 ± 0.0043	-39.8 ± 6.5	6.8842 ± 0.0087	HARPS-N
392.57382	35.5504 ± 0.0055	-18.9 ± 8.2	6.8885 ± 0.0109	HARPS-N
393.33790	35.5809 ± 0.0066	-3.2 ± 10.0	6.8780 ± 0.0133	HARPS-N
393.47098	35.6069 ± 0.0056	-37.6 ± 8.4	6.8795 ± 0.0111	HARPS-N
394.35486	35.6925 ± 0.0042	-32.3 ± 6.4	6.8701 ± 0.0085	HARPS-N
394.54090	35.7050 ± 0.0054	-45.8 ± 8.1	6.8717 ± 0.0108	HARPS-N
395.41956	35.6694 ± 0.0165	3.9 ± 24.7	6.8693 ± 0.0329	HARPS-N
396.44205	35.493 ± 0.042	-24.5 ± 75.1	9.682 ± 0.104	SOPHIE
398.39484	35.582 ± 0.010	-35.3 ± 18.2	9.523 ± 0.025	SOPHIE
399.41136	35.554 ± 0.038	-18.1 ± 67.9	9.415 ± 0.094	SOPHIE
400.38519	35.435 ± 0.019	-47.5 ± 33.5	9.517 ± 0.046	SOPHIE
401.35244	35.448 ± 0.016	-22.0 ± 29.3	9.572 ± 0.040	SOPHIE
402.34190	35.553 ± 0.011	-2.7 ± 19.6	9.540 ± 0.027	SOPHIE
404.43149	35.436 ± 0.019	-11.0 ± 34.0	9.591 ± 0.047	SOPHIE

Notes. MBJD = Modified Barycentric Julian Date (BJD-2457000)

Table A.4. Radial velocity data for EPIC-212110888

MBJD (days)	RV (km/s)	BIS (m/s)	FWHM (km/s)	Instrument
381.59795	45.863 ± 0.040	-70 ± 65	10.597 ± 0.080	CAFE
382.62804	46.167 ± 0.049	-178 ± 70	10.841 ± 0.110	CAFE
392.60905	46.5458 ± 0.0034	35.3 ± 5.1	9.5015 ± 0.0069	HARPS-N
393.50729	46.2009 ± 0.0133	40.7 ± 19.9	9.4696 ± 0.0266	HARPS-N
394.61995	46.4477 ± 0.0138	36.6 ± 20.8	9.4864 ± 0.0277	HARPS-N
398.43529	46.490 ± 0.018	11 ± 32	11.395 ± 0.044	SOPHIE
399.44751	46.136 ± 0.018	-17 ± 32	11.437 ± 0.045	SOPHIE
399.68876	46.109 ± 0.014	51 ± 25	11.554 ± 0.035	SOPHIE
403.49977	46.328 ± 0.019	16 ± 33	11.367 ± 0.046	SOPHIE

Notes. MBJD = Modified Barycentric Julian Date (BJD-2457000)

Appendix A: Additional tables and figures

Table A.6. Photometry used for the spectral energy distribution analysis of EPIC-210957318 and EPIC-212110888

Band	EPIC-318	EPIC-888
Johnson-V	13.53 ± 0.039	11.548 ± 0.057
Johnson-B	14.506 ± 0.030	12.429 ± 0.033
g'	-	11.892 ± 0.119
r'	13.184 ± 0.042	11.389 ± 0.026
i'	12.819 ± 0.046	11.264 ± 0.038
2MASS-J	11.632 ± 0.019	10.528 ± 0.025
2MASS-H	11.190 ± 0.016	10.258 ± 0.022
2MASS-Ks	11.088 ± 0.020	10.193 ± 0.017
WISE-W1	11.016 ± 0.023	10.174 ± 0.023
WISE-W2	11.058 ± 0.021	10.207 ± 0.020
WISE-W3	11.067 ± 0.161	10.159 ± 0.169

Notes. Optical magnitudes (Johnson-V, Johnson-B, g', r', and i') were obtained from the APASS database. Infrared values were obtained from Cutri et al. (2013).

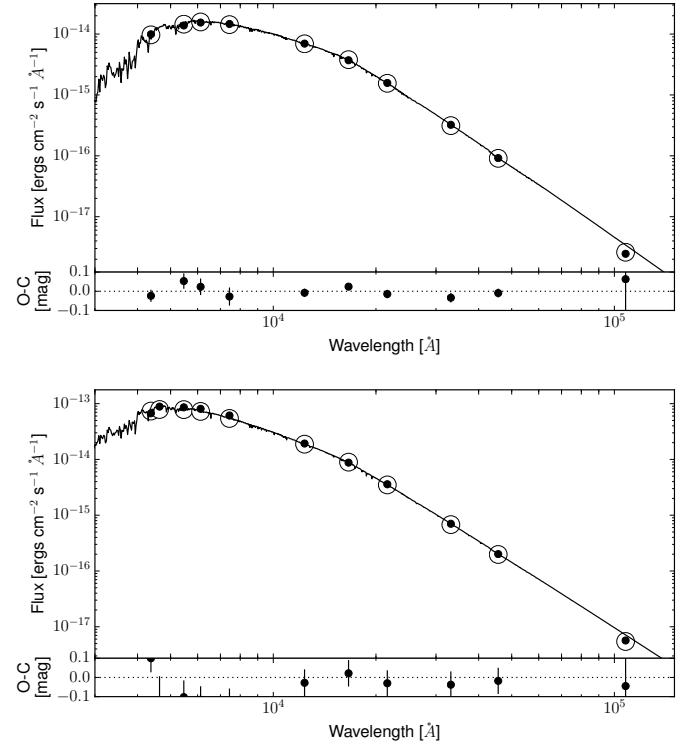
**Fig. A.1.** Results of the SED fitting in the joint analysis of the data with PASTIS for EPIC-318 (top panel) and EPIC-888 (bottom panel). The final models are shown with solid lines and the residuals of the data are presented in the lower part of each panel.

Table A.5. List of free parameters used in the PASTIS analysis of the light curves, radial velocities and SED with their associated prior.

Parameter	EPIC-318	EPIC-888
<i>Orbital parameters</i>		
Orbital period P [d]	$\mathcal{N}(4.09803; 1 \times 10^{-3})$	$\mathcal{N}(2.996; 1 \times 10^{-3})$
Epoch of first transit T_0 [BJD _{TDB}] - 2450000	$\mathcal{N}(7063.826; 0.1)$	$\mathcal{N}(7141.35; 0.1)$
Orbital eccentricity e	$\beta(0.867; 3.03)$	0 (fixed)
Argument of periastron ω [°]	$\mathcal{U}(0; 360)$	–
Inclination i [°]	$\mathcal{S}(70; 90)$	$\mathcal{S}(70; 90)$
<i>Planetary parameters</i>		
Radial velocity amplitude K [m/s]	$\mathcal{U}(0; 1000)$	$\mathcal{U}(0; 1000)$
Planet-to-star radius ratio a/R_\star	$\mathcal{U}(0; 0.5)$	$\mathcal{U}(0; 0.5)$
<i>Stellar parameters</i>		
Effective temperature T_{eff} [K]	$\mathcal{N}(5573; 38)$	$\mathcal{N}(6139; 50)$
Surface gravity $\log g$ [g/cm ²]	$\mathcal{N}(4.32; 0.20)$	$\mathcal{N}(4.07; 0.21)$
Iron abundance [Fe/H] [dex]	$\mathcal{N}(0.14; 0.03)$	$\mathcal{N}(0.11; 0.04)$
Reddening E(B-V) [mag]	$\mathcal{U}(0; 1)$	$\mathcal{U}(0; 1)$
Systemic radial velocity V_{sys} [km/s]	$\mathcal{U}(-100, 100)$	$\mathcal{U}(-100, 100)$
Distance to Earth d [pc]	$\mathcal{P}(2; 10; 1000)$	$\mathcal{P}(2; 10; 1000)$
Linear limb darkening coefficient u_a	$\mathcal{U}(0, 1.2)$	$\mathcal{U}(0, 1.2)$
Quadratic limb darkening coefficient u_b	$\mathcal{U}(0, 1.2)$	$\mathcal{U}(0, 1.2)$
<i>Instrumental parameters</i>		
CAFE radial velocity jitter $\sigma_{\text{RV,CAFE}}$ [m/s]	–	$\mathcal{U}(0; 100)$
SOPHIE radial velocity jitter $\sigma_{\text{RV,SOPHIE}}$ [m/s]	$\mathcal{U}(0; 100)$	$\mathcal{U}(0; 100)$
HARPS-N radial velocity jitter $\sigma_{\text{RV,HARPS-N}}$ [m/s]	$\mathcal{U}(0; 100)$	$\mathcal{U}(0; 100)$
CAFE – SOPHIE radial velocity offset $\Delta \text{RV}_{S,\text{CAFE}}$ [m/s]	$\mathcal{U}(-1000; 1000)$	$\mathcal{U}(-1000; 1000)$
HARPS-N – SOPHIE radial velocity offset $\Delta \text{RV}_{S,H-N}$ [m/s]	$\mathcal{U}(-1000; 1000)$	$\mathcal{U}(-1000; 1000)$
SED jitter σ_{SED} [mag]	$\mathcal{U}(0; 1)$	$\mathcal{U}(0; 1)$

Notes. $\mathcal{N}(\mu; \sigma^2)$ is a normal distribution with mean μ and width σ^2 , $\mathcal{U}(a; b)$ is a uniform distribution between a and b , $\mathcal{S}(a, b)$ is a sine distribution between a and b , $\beta(a; b)$ is a Beta distribution with parameters a and b , and $\mathcal{P}(n; a; b)$ is a power-law distribution of exponent n between a and b .

References. The choice of prior for the orbital eccentricity is described in Kipping (2013).

Table A.7. Host star, planet and orbital parameters inferred from the joint analysis of the data. Uncertainties represent the 15.7% and 84.3% percentiles of the marginalized posterior distribution

Parameter	EPIC 318	EPIC 888
Planet properties		
K (m/s)	79.9 ± 4.0	209 ± 12
R_p/R_\star	0.1302 ± 0.0026	0.0905 ± 0.0017
M_p (M_{Jup})	0.623 ± 0.031	1.76 ± 0.13
R_p (R_{Jup})	1.196 ± 0.060	1.350 ± 0.067
ρ_p (ρ_{Jup})	0.364 ± 0.058	0.71 ± 0.11
T_{eq} (K)	1185^{+44}_{-28}	1742 ± 38
Orbital properties		
Period (days)	4.098507 ± 0.000028	2.995607 ± 0.000017
T_0 (MBJD ^a , days)	63.80710 ± 0.00027	141.35132 ± 0.00022
i (deg)	86.32 ± 0.38	82.06 ± 0.51
e	$0.027^{+0.036}_{-0.020}$	0.0 (assumed)
ω (deg)	120^{+100}_{-51}	-
a (au)	0.04986 ± 0.00035	$0.04419^{+0.00063}_{-0.00110}$
a/R_\star	11.40 ± 0.52	6.20 ± 0.25
b_{primary}	0.721 ± 0.036	0.857 ± 0.023
T_{dur} (hours)	2.355 ± 0.030	2.492 ± 0.023
Host properties		
M_\star (M_\odot)	0.984 ± 0.020	$1.281^{+0.055}_{-0.091}$
R_\star (R_\odot)	0.941 ± 0.041	1.526 ± 0.076
ρ_\star (ρ_\odot)	1.18 ± 0.15	0.356 ± 0.044
V_{sys} (km/s)	35.5090 ± 0.0087	46.311 ± 0.013
d (pc)	323 ± 14	377 ± 20
E(B-V)	0.253 ± 0.014	0.036 ± 0.020
$\log g$ (cgs)	4.484 ± 0.042	4.173 ± 0.032
T_{eff}	5581 ± 38	6132 ± 47
[Fe/H] (dex)	0.136 ± 0.029	0.24 ± 0.22
$\log L/L_\odot$ (dex)	-0.112 ± 0.039	0.471 ± 0.048
ua	0.24 ± 0.18	$0.18^{+0.20}_{-0.13}$
ub	0.34 ± 0.28	0.28 ± 0.28
$v \sin i$ (km/s)	3.9 ± 1.1	5.2 ± 1.4
Jitters (σ) and instrumental offsets (ΔRV)		
$\sigma_{\text{RV,HARPS-N}}$ (m/s)	$3.6^{+4.8}_{-2.5}$	16^{+29}_{11}
$\sigma_{\text{RV,SOPHIE}}$ (m/s)	$10.3^{+13.0}_{-7.2}$	$13.2^{+22.0}_{-9.5}$
$\sigma_{\text{RV,CAFE}}$ (m/s)	-	43 ± 21
$\Delta RV_{S,H-N}$ (m/s)	-121.5 ± 9.1	-81 ± 26
$\Delta RV_{S,CAFE}$ (m/s)	-	228 ± 50
σ_{K2} (ppm)	385 ± 18	188.3 ± 7.3
σ_{SED} (mag)	$0.016^{+0.016}_{-0.011}$	$0.065^{+0.032}_{-0.021}$
K2 contamination	$0.032^{+0.036}_{-0.023}$	$0.025^{+0.031}_{-0.018}$

Notes. ^(a) Modified Barycentric Julian Date = BJD-2457000 (days)